IEEE Access
Multidisciplinary | Rapid Review | Open Access Journal

Received August 10, 2020, accepted September 11, 2020, date of publication September 18, 2020,
date of current version September 30, 2020.

Digital Object Identifier 10.1109/ACCESS.2020.3024636

Conformal and Ultra Shallow Junction Formation Achieved Using a Pulsed-Laser Annealing Process Integrated With a Modified Plasma Assisted Doping Method

SEUNGHUN BAIK[1], DONG-JAE KWON[1], HONGKI KANG[1], JAE EUN JANG[1], (Member, IEEE), JAEWON JANG[2,3], (Member, IEEE), Y. S. KIM[4,5], AND HYUK-JUN KWON[1,6]

[1]Department of Information and Communication Engineering, Daegu Gyeongbuk Institute of Science and Technology (DGIST), Daegu 42988, South Korea
[2]School of Electronics Engineering, Kyungpook National University, Daegu 41566, South Korea
[3]School of Electronic and Electrical Engineering, Kyungpook National University, Daegu 41566, South Korea
[4]Lam Research Corporation, Fremont, CA 94538, USA
[5]SEMES, Hwaseong 18383, South Korea
[6]Convergence Research Advanced Centre for Olfaction, Daegu Gyeongbuk Institute of Science and Technology (DGIST), Daegu 42988, South Korea

Corresponding authors: Y. S. Kim (ys.kim@lamresearch.com) and Hyuk-Jun Kwon (hj.kwon@dgist.ac.kr)

This work was supported in part by the Basic Science Research Program through the National Research Foundation of Korea (NRF) funded by the Ministry of Science and ICT (MSIT) under Grant 2019R1F1A1061883 and Grant 2019M3C1B8090840, and funded by the Ministry of Education under Grant 2020R1A6A1A03040516, and in part by the DGIST Research and Development Program of MSIT under Grant 19-CoE-BT-03.

ABSTRACT Recently, a shallow and conformal doping profile is required for promising 3D structured devices. In this study, we deposited the dopant phosphorus (P) using modified plasma assisted doping (PaD) followed by an annealing process to electrically activate the dopants. A rapid thermal annealing process (RTP) was the first approach tested for activation but it resulted in a deep junction ($>$ 35 nm). To reduce the junction depth, we tried the flash lamp annealing process (FLP) to shorten the annealing time. We also predicted the annealing temperature by numerical thermal analysis, which reached 1,020 °C. However, the FLP resulted in a deep junction ($\sim$ 30 nm), which was not shallow enough to suppress short channel effects. Since an even shorter annealing process was required to form a ultra-shallow junction, we tried the laser annealing process (LAP) as a promising alternative. The LAP, which had a power density of 0.3 J/cm^2, increased the surface temperature up to 1,100 °C with a shallow isothermal layer. Using the LAP, we achieved a USJ with an activated surface dopant concentration of 3.86×10^{19} cm^{-3} and a junction depth of 10 nm, which will allow further scaling-down of devices.

INDEX TERMS Ultra-shallow junction, phosphorus, plasma assisted doping, laser annealing process.

I. INTRODUCTION

Over the last few decades, users' demands and a price war among semiconductor industries have been driving the continuous scaling-down of electronic devices. Reducing the channel length from 45 nm to 10 nm made it possible to fabricate 13 times more devices from the same sized wafer, and with enhanced performance. However, shrinking the size of the devices in planar direction reached its limitation and could not afford the further improvements in 2D. As a result, it led the device architecture to move on non-planar and 3D structures.

The associate editor coordinating the review of this manuscript and approving it for publication was Jenny Mahoney.

There are several device structures proposed and realized in 3D such as FinFET, 3D NAND, 4F^2 DRAM with 3D vertical gate and future device structures [1]–[6]. Device structures in 3D seem to allow further scaling down and boosted performances, but it also forced the fabrication processes to be adapted. 3D channel and contact in a non-planar device, for example FinFET and gate-all-around (GAA) devices, require conformal and shallow doping profiles [7]. Especially, the contact requires ultra-shallow junction (USJ) to overcome short channel effect (SCE) and high dose for low resistances. NAND architecture is also moving to 3D because stacking structure is less affected by SCE and parasitic capacitance with higher stability [8]. To achieve 3D stacking of NAND, vertical gate array and embedded common source

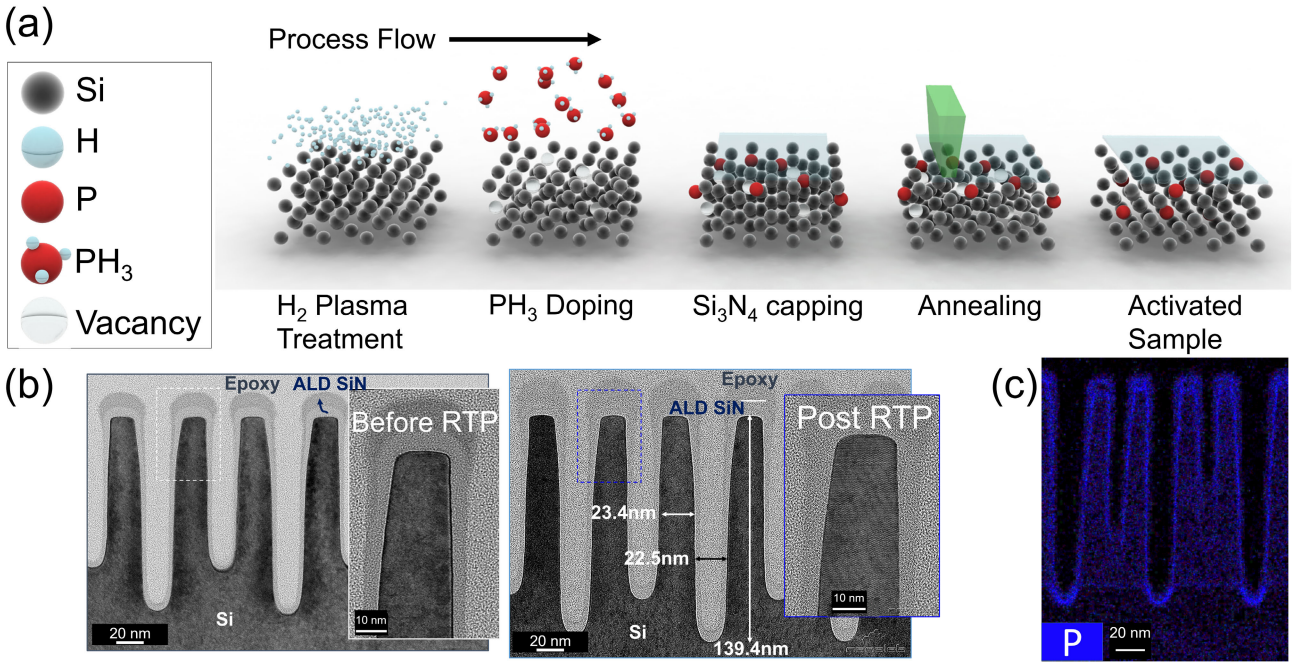

FIGURE 1. (a) Schematic diagram of fabrication process flow. (b) The TEM image of the high aspect ratio (6:1) fin array (black); the figures at left-side show fin array without any process including PaD and RTP while the right-side is the result after PaD and RTP. The narrowest gap between the fins is 22.5 nm long. The fin width is about 23.4 nm thick and the maximum height is about 139.4 nm. There were no structural damage or lattice distortions. (c) The EDS result after PaD shows that P dopants were conformally deposited .

line (CSL) of 3D NAND needs to be conformally and uniformly doped. The memory device also faced a limitation for reducing cell size. The trial to move from $6F^2$ to $4F^2$ DRAM to reduce the cell size by 33 % also demands conformal and shallow doping of n-type dopants to generate source and drain under buried bit-line with assisted hole-draining. Therefore, to reach the next stage on the technology roadmaps (beyond 10 nm node), highly doped regions with shallow doping profiles are necessary.

As the device structures become smaller and move to 3D, conventional doping methods are not capable of fully meeting the doping requirements. Ion shading (shadowing effect), surface penetration issues (channeling) and surface bombardment damage are unavoidable with ion implantation processes because the ions are injected with a fixed incident angle and directionality with relatively high driving energy [9]–[12]. Another doping method, plasma doping (PLAD), uses high density plasma reactors at low energy, under 500 eV, to produce relatively shallow doping profiles with reduced crystalline damage [13], [14]. However, PLAD is unable to form a uniform conformal doping profile because of its bias power. The bias power imparts directionality to the dopants, and as a result, vertical doping profiles form deeper doping than lateral doping. The limitations of these conventional doping processes lead to non-uniform doping and source/drain current problems, resulting in lower reliability. To overcome these limitations, we modified the plasma assisted doping (PaD) method by removing the bias power in order to eliminate damage that is concentrated near the Si substrate and make the dopant profile shallower and abrupt.

Furthermore, to activate the dopants and make them electrically effective, subsequent annealing is required after a dopant delivery. The most widely used annealing process is a rapid thermal annealing process (RTP). However, this method also makes the junction deeper because the dopant diffuses proportionally further with annealing time. As alternative methods, we also studied the flash lamp annealing process (FLP) and laser annealing process (LAP), which have relatively shorter process times and higher energy density, to reduce annealing time and the diffusion of dopants to form an abrupt and shallow junction [15]–[17].

Among these various annealing methods, laser annealing with a short pulse duration can minimize dopant diffusion. Shorter annealing times have advantages in terms of diffusion depth and higher peak power effects. Moreover, the short pulse delivers energy on a timescale of electron-phonon scattering for thermal vibration and coupling relaxation (10^{-10} s for thermal diffusion and 10^{-12} s for carrier-phonon scattering) [18]. The short-pulsed process delivers energy without thermal transfer or with a minimum amount of heat.

II. EXPERIMENTAL

A. PaD METHOD

Fig. 1a illustrates the overall scheme of our proposed PaD process. Note that overall PaD was processed by a transformer coupled plasma (TCP) reactor to uniformly generate ions and radicals. First, H_2 plasma treatment was conducted on a p-type Si (100) substrate. A power of 300 W was applied for the source power without a bias power under H_2 (350 sccm) and Ar (50 sccm) gases and the chamber

pressure was 10 mTorr during the process for 60 seconds. The substrate was heated to 330 °C to minimize Si surface damage by regrowing the amorphized surface. The effects of H_2 plasma treatment on a Si substrate have been widely reported [19]–[21]. Here, the H_2 plasma treatment was used to enhance the doping level in our process; H_2 plasma treatment of the Si bulk increased the number of vacancies at the very near surface (∼30 nm) and the dopants diffused via these vacancies into the Si [22]–[26]. Thus, more vacancies near the surface helped dopants to occupy Si lattice sites with lower energy. The enhanced doping profile compared to no H_2 plasma treatment is included in Fig. S1 in the supplementary materials. In addition, H_2 plasma treatment has several advantages. It is effective for cleaning the surface and it removes residual F from HF dipping for native oxide removal. In the supplementary materials S4, additional Electron Energy Loss Spectroscopy (EELS) figures are provided for the result. H_2 plasma treatment also prevented re-oxidation of the Si surface.

Second, to deliver phosphorus (P) atoms as the dopants, we used gaseous PH_3 (45 sccm), Ar (50 sccm), and He (450 sccm) gases for the plasma process with low energy and a high dose and the process time was 60 seconds. The RF bias was removed for USJ formation without structure damages while only the source power of 1,500 W was applied. The chamber temperature was maintained at 330 °C. The chamber pressure was controlled for 10 mTorr. Our PaD process is very different from conventional PLAD, which impacts the surface with high ion energy. In the PaD, even though the bias voltage has been removed, more vacancies created by H_2 plasma treatment (previous step) help the PaD process to deliver dopants because dopants diffuse through defects such as vacancies. Also, removing the bias voltage during the dopant delivery process enables shallower dopant profiles, which allows the formation of sub-10 nm shallow junctions. The measured result of the PaD processing is included in Fig. S2 (the supplementary materials).

After the dopant delivery, a Si_3N_4 film was deposited on the surface using the plasma enhanced atomic layer deposition process (PE-ALD) without a vacuum break, which guaranteed that there were no contamination or pollution issues. SiH_4 (30 sccm), Ar (50 sccm), and N_2 (300 sccm) were used as reactive gases to deposit Si_3N_4 layer. The RF power was removed and only the source power of 300 W was given. The chamber pressure was maintained for 5 mTorr and the temperature was maintained for 330 °C. The process time was taken for 5 seconds and it was repeated for 15 times to deposit a 5 to 10 nm thick Si_3N_4 layer. It is well known that the out-diffusion of P during the doping process is a critical problem [27]. To address this issue, the Si_3N_4 film was applied as a capping layer to prevent the out-diffusion of dopants during the annealing process. A transmission electron microscopy (TEM) image is provided in Fig. S3 in the supplementary materials. A subsequent annealing process was then conducted to electrically activate the dopants. The overall PaD process of H_2 plasma treatment and Si_3N_4 capping layer deposition successfully prevented carbon contamination (Fig. S4 in the supplementary materials).

B. CONFORMALITY TEST FOR PaD PROCESS

As the trend of FET structures creates a 3D geometry in logical NAND flash memory and logic front-end-of-line (FEOL) [28], [29], we tested the conformality of our PaD method in the 3D Si fin structure with a high aspect ratio of 6:1. Fig. 1b shows the TEM image of the 3D test structure with Si_3N_4 capping layer before annealing process, which is the last step of the PaD process (the left-side image), and after RTP (the right-side image). The fin width is about 23.4 nm thick and the maximum height is about 139.4 nm. The fin arrays are fabricated for the test of conformality. In the ion implantation process, the conventional dopant delivery process typically results in surface damage, as mentioned above. Comparing the structures in Fig. 1b, no Si structure damage or loss can be seen after both the PaD process and the annealing process (RTP at 950 °C for 10 s). The fin edges are definite without collapse and the boundary between the Si and Si_3N_4 films can be clearly seen. This confirms that the overall PaD and annealing processes applied after H_2 plasma treatment were free of damage; in our PaD method, plasma energy made by the source power only decoupled ions and it did not deteriorate the 3D structures.

Since PaD is also advantageous for fabricating high aspect ratio 3D structures, we additionally demonstrated a conformal doping profile with P. In Fig 1c, the mapping result of Energy-dispersive X-ray spectroscopy (EDS) shows that the PaD delivered the dopants to the surface of the sample appropriately with a uniform and conformal formation, and there were no problems with dopant depth control, without bias power. The dopants were delivered properly even for the bottom of a deep trench. An additional EDS result is in Fig. S5 of the supplementary materials.

III. RESULTS AND DISCUSSION

A. RAPID THERMAL PROCESS (RTP)

Our first attempt to activate the dopants involved the use of RTP, which is the most commonly employed method. Fig 2a presents the secondary ion mass spectrometry (SIMS) results for various RTP conditions. Here, we note that 3D structured samples with high aspect ratio allowed to test the conditions for the processes, PaD and annealing steps, to deliver and dope the dopants conformally. However, 3D structure limited the reliable evaluations for electrical and quantitative analyses. Therefore, results for electrical measurements and USJ profiles were obtained from planar structured samples due to the accuracy of the quantitative analysis. The starting point (0 nm) of the SIMS analysis is where the intensity of Si becomes higher than 95 %, which is the surface of the Si sample. The sample was sputtered with Ar ions for depth profiling. As the Ar ions collided with the surface, they created craters and removed the surface atoms. Therefore, during the SIMS analysis, sputtering process removes the

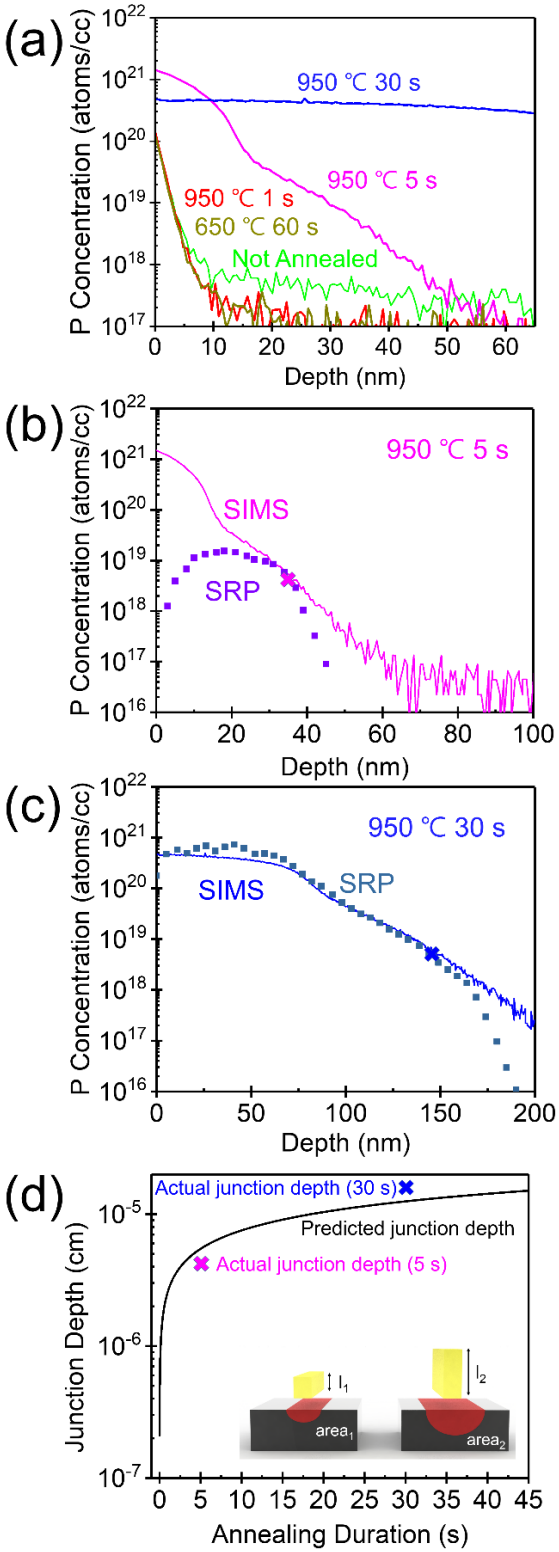

FIGURE 2. (a) SIMS profiles for RTP process conditions. (b) SRP profile compared with SIMS profile for RTP of 5 s at 950 °C. (c) SRP profile compared with SIMS profile for RTP of 30 s at 950 °C. (d) Theoretically predicted junction depth in different annealing durations. The magenta cross and the blue cross represent the annealing duration of 5 seconds and 30 seconds each. The inset figures briefly show the relation between the annealing duration and heat effective area.

capping layer allowing the sample to be analyzed by depth profiling [30].

Fig. 2a shows that both the annealing conditions of 650 °C for 60 s (dark green line) and 950 °C for 1 s (red line) have doping profiles similar to the sample before annealing, which indicated that using a higher temperature shortened the annealing time. It also means that the diffusion might not be effective when the sample is annealed for too short a time or at low temperature. However, the surface dopant concentration was still limited at around 1×10^{20} cm^{-3}. When we increased the annealing duration to 5 s with the annealing temperature fixed at 950 °C, the dopants started to form a higher surface dopant concentration. The longer duration RTP (which was increased up to 30 s) resulted in deeper diffusion, which limited the formation of a USJ.

A spreading resistance profiling (SRP) profile is shown in Fig. 2b, which illustrates the electrically activated dopant concentration profile with depth profiling for samples prepared with RTP for 5 s at 950 °C, along with the SIMS result. In contrast to the SIMS profiles, as the SRP suggests, the dopants were not fully activated. SIMS detects the physical quantity of dopant atoms, which is the maximum amount available for activation. The kink trend is found in the result, which might indicate that there are vacancies, which are created by H_2 plasma treatment. There are two major diffusion routes of phosphorus in silicon. At a higher concentration of P, vacancy mediated diffusion is dominant for dopants. At a lower concentration of P, the diffusion is mostly caused by self-interstitials [22], [23], [31], [32]. Here, as the H_2 plasma treatment created many more vacancies near the surface, a short RTP duration of 5 seconds was not fully effective to heal the Si lattice and remove vacancies, which possibly resulted in the kink trend. The highest dopant concentration (2×10^{19} cm^{-3}) was reached at 20 nm beneath the surface, while the surface dopant concentration was limited to 1×10^{18} cm^{-3}. This is significant because the highest dopant concentration is generally found at the surface.

This lower surface dopant concentration might be due to various reasons. First, it could have been caused by deactivation of dopants, which means that some of dopants were possibly deactivated because of the short RTP. However, note that the doping level was higher than the samples that were not treated. This seems to indicate that there is a limitation in shortening the annealing duration of the RTP. The other reason for the low surface concentration level could be the probe separation distance resulting from the configuration of the SRP hardware [33]. When the probe separation distance is in the range of 2 to 5 times the distance to the insulating layer, distortions may appear in the surface dopant concentration. Another possible reason for the lower surface dopant concentration could be from damage caused to the surface by beveling the sample. To bevel the sample, a damaging process is involved, and such damage has been reported to influence dopant concentration results [34]–[37].

Fig. 2c shows the SRP profile of a sample prepared by the RTP for 30 seconds at 950 °C, along with the SIMS

result, which is the blue line in Fig 2a. As the annealing duration becomes longer, the dopants are electrically well activated. Note that the longer annealing process was a trade-off because the dopants diffused deeper, and the junction depth increased (> 100 nm). There were negligible errors in Fig. 2c in which the maximum SRP value exceeded the SIMS maximum value. The error was found at the surface region but none of the errors were seen below a depth of 70 nm.

To understand the diffusion depth, the diffusion profile following the shallow pre-deposition step and the drive-in diffusion step should be considered. In this study we used PaD: the pre-deposition step delivered dopants, while the drive-in diffusion step (RTP, FLP, and LAP) placed and activated the dopants in the Si lattice. Assuming a constant dose of dopants, we describe the final diffusion profile by the equation below [38]:

$$\mathrm{C}\,(\mathrm{x}) = \left(\frac{2C_0}{\pi}\right) \cdot \left(\frac{D_1 t_1}{D_2 t_2}\right)^{\frac{1}{2}} \cdot e^{\frac{-x^2}{4D_2 t_2}} \tag{1}$$

where C(x) is the dopant concentration at depth x, C_0 is the surface dopant concentration before the annealing process, D_1 is the diffusion constant at the pre-deposition temperature, t_1 the pre-deposition time, D_2 is the diffusion constant at the drive-in (annealing) temperature, and t_2 is the drive-in time. From the equation, the junction depth is derived when C(x) meets the Si background concentration (5×10^{18} cm^{-3}) as below:

$$x_j = \sqrt{4D_2 t_2 \ln\left(\frac{2C_0\sqrt{D_1 t_1}}{5 \times 10^{18} \cdot \pi\sqrt{D_2 t_2}}\right)} \tag{2}$$

Because the PaD process was used with fixed parameters for the pre-deposition process, $D_1 t_1$ can be considered a fixed constant value, and then the final junction depth can be determined as a function of D_2 and t_2 which are determined by the annealing process (RTP, FLP and LAP). Since the diffusion constant is dependent on the temperature, this equation can also explain why the processes at 650 °C, 60 s and 950 °C, 1s show similar doping profiles.

In Fig. 2d, the theoretical junction depth was calculated from equation (2), and the magenta and blue points marked on the graph are the expected junction depths for 5 s and 30 s, respectively. Our experimental results agreed with the theoretical values, thus confirming that reducing the annealing duration is a very successful approach for making a smaller heat effective area. For the additional electrical results, sheet resistance results are plotted versus junction depth in supplementary materials, Fig. S6.

The thermal penetration depth has the relation $d_{th} \approx \alpha\sqrt{D\tau}$ (where the d_{th} stands for the thermal penetration depth, α for the transient heating coefficient, D for thermal diffusivity, and τ for the annealing time) [39]. We chose $\alpha = 2$ to describe the 1/e (spatial) decay in the temperature distribution, which is a general solution of the linear heat equation for a point source in infinite space in case of transient heating. The inset in Fig. 2d helps explain the phenomena. The two different durations, l_1 and l_2 ($l_1 < l_2$), each generated a heat effective area with sufficient energy for doping (diffusion and activation). The energy absorbed in the annealing processes is converted to local heat and diffuses by thermal conduction via scattered thermal vibrations. The area has a dominant effect on the doping profile since the dopants diffuse by the energy mostly given by thermal sources. Because the lamp duration of l_2 is longer than l_1, the heat diffused deeper, made a larger red heated area and the dopants diffused deeper ($area_1 < area_2$). Here, the solution for effectively fabricating a shallow junction could be shortening the annealing process time, but the RTP process time cannot be reduced below a certain limit, where it only raises the temperature by 400 °C/s [40].

B. FLASH LAMP ANNEALING PROCESS (FLP)

To make the junction shallower, for the next attempt to reduce annealing time we investigated FLP with a Xe lamp. There were huge differences in temperature between the surface and the bottom, caused by the short lamp duration (10-20 ms), which was unlike in the RTP (process time: 1-150 s). Here, note that the differentiating feature of the FLP (a sudden temperature increase and large temperature difference between the surface and the bottom) may cause non-negligible thermal stress which results in cracking or damage to the wafer. Thus, we preheated the samples at 300 °C and 400 °C to mitigate the thermal stress. As the FLP SIMS results show in Fig. 3a, the green line (preheating temperature: 300 °C, lamp duration: 20ms, energy density: 80 J/cm^2) resulted in a poor surface dopant concentration (<1×10^{19} cm^{-3}). This means that the energy density was too low to drive in the dopants. On the other hand, the cyan (300 °C, 20 ms, 88 J/cm^2) and magenta (300 °C, 10 ms, 127 J/cm^2) lines reveal better profiles; the surface dopant concentration of the cyan and magenta lines reached higher than 4×10^{20} cm^{-3} and had a very steeply sloping doping profile.

Note that the magenta line indicates a higher energy density and shorter lamp duration compared to the cyan line. The FLP with higher energy density produced a similar SIMS profile even with a shorter annealing duration; this can also be understood from equation (1). Accordingly, we increased the base temperature (400 °C) and lamp duration (20 ms) to achieve higher doping effects.

At the same time, the orange (400 °C, 20 ms, 80 J/cm^2) line met the low surface concentration (<1×10^{19} cm^{-3}), so we studied FLP conditions with higher energy density. Under those conditions, the blue (400 °C, 20 ms, 120 J/cm^2) and the red (400 °C, 20 ms, 127 J/cm^2) lines showed the most favorable results. The blue and the red lines exhibited the highest surface concentration (~2×10^{21} cm^{-3}). As the sheet resistance indicates the activation of dopants and the red line showed the lowest sheet resistance results, we selected the red line conditions, preheating of 400 °C, lamp duration of 20 ms and the energy density of 127 J/cm^2, as the best FLP conditions.

Fig. 3b shows the SRP profile for the best conditions, preheating of 400 °C, a lamp duration of 20 ms and an

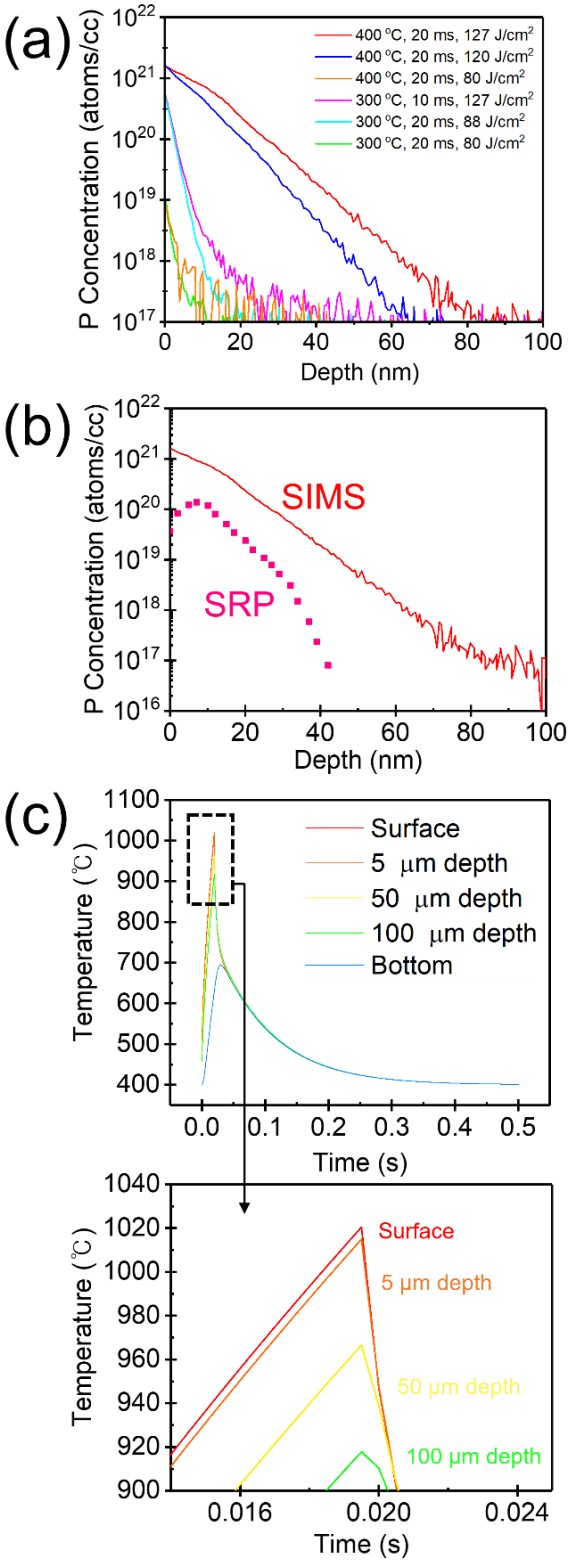

FIGURE 3. (a) SIMS profiles for FLP process conditions. (b) SRP profile compared with SIMS profile for FLP of preheating at 400 °C, lamp duration of 20 ms and energy density of 127 J/cm^2. (c) Thermal simulation (COMSOL Multiphysics) result for FLP of preheating at 400 °C, lamp duration of 20 ms and energy density of 127 J/cm^2.

energy density of 127 J/cm^2, which is the red line in Fig. 3a, compared to the SIMS result. Compared to the junction depth produced by the RTP, the SRP profile had the highest activated dopant concentration of about 1.37×10^{20} cm^{-3}. The shallowest junction depth, where the concentration of P reached 5×10^{18} cm^{-3}, was 30 nm. The FLP results indicated that it could potentially form an effective shallow junction. However, the junction depth is still limited to the tens of nm scale, while a sub-10 nm scale is required for future device technology [41].

The temperature profile generated during the FLP was predicted by numerical thermal analysis using COMSOL Multiphysics. Because the flash lamp located inside the chamber was perfectly covered, direct measurement was very challenging. Here, we note that our theoretical equation model was applied to the equilibrium temperature approximation. While temperature equilibrium (*i.e.,* electron–phonon coupling) typically occurs within the range of 10^{-12}-10^{-10} seconds, this approximation is reasonable because our FLP takes a relatively long duration (10-20 ms).

The simulation results for the generated temperature changed over time at the surface. The results for 5 μm, 50 μm, and 100 μm beneath the surface and the bottom of the substrate (800 μm thick) are plotted in Fig. 3c. The graph above in Fig. 3c presents the overall temperature changes, while the graph below shows the peak points of the highest temperature in more detail. According to the predicted results, the FLP with the red conditions (400 °C, 20 ms, 127 J/cm^2) can raise the temperature of the surface to nearly 1,020 °C; the temperature transition only took 0.02 s, and there was only a little time delay (0.04 s) in the heat flow from the surface to the bottom. The above graph shows that there is a relatively thick isothermal layer (surface $\sim$ 5 μm) which has a temperature similar to the surface. This indicates that the dopants near the isothermal layer were diffused and activated by the thermal energy. As a result, we can see in Fig. 3b that the junction depth for the FLP was 30 nm, and the P concentration dropped very sharply at a depth of 40 nm, which is still not shallow enough.

C. LASER ANNEALING PROCESS (LAP)

To make a USJ, we investigated the LAP as an alternative approach. We preheated the wafer with the RTP at 650 °C for 60 s; this increased the surface temperature, but it was not enough energy to cause the dopants to diffuse. A laser beam with a wavelength of 532 nm and a pulse duration of 50 ns was shaped to 0.1 mm $\times$ 1.0 mm. A pulsed laser delivered energy within a very short time period, creating a high peak power effect, and the peak power raised the temperature very high compared to the degree produced by average power.

The SIMS results for the LAP, while the energy density of the laser beam was swept from 0.25 J/cm^2 to 0.3 J/cm^2, are plotted in Fig. 4a. The red (0.25 J/cm^2) and the magenta (0.26 J/cm^2) lines show the surface dopant concentrations of 1.07×10^{21} cm^{-3} and 8.24×10^{20} cm^{-3}, respectively. As the energy density increased, the cyan (0.295 J/cm^2) and the blue (0.3 J/cm^2) lines exhibited higher surface dopant

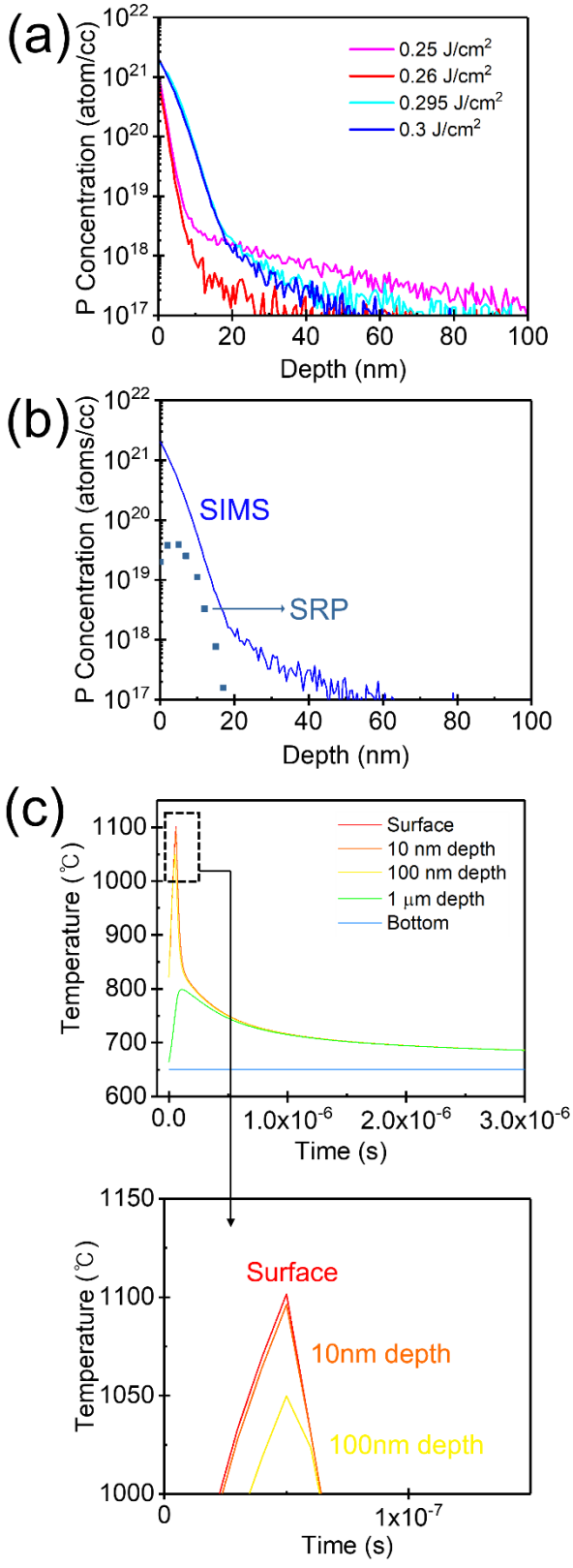

FIGURE 4. (a) SIMS profiles for LAP process conditions. (b) SRP profile compared with SIMS profile for LAP (0.3 J/cm^2). The junction depth was about 10 nm. (c) Thermal simulation (COMSOL Multiphysics) result for LAP for energy density of 0.3 J/cm^2. LAP would increase the surface temperature to 1,100 °C in very short time (50 ns) with a shallow isothermal layer (10 nm).

concentrations of 1.88×10^{21} cm^{-3} and 2.02×10^{21} cm^{-3}, respectively.

In Fig. 4b, indicated by the blue line, the SRP profile for the LAP with an energy density of 0.3 J/cm^2, which represents the highest surface dopant concentration in Fig. 4a, is compared to the SIMS result. The SRP profile had a highest activated dopant concentration of about 3.86×10^{19} cm^{-3} and the junction depth where the P concentration reached 5×10^{18} cm^{-3} was 10 nm. The LAP successfully formed the USJ while the RTP and FLP did not. Since the LAP with an energy density of 0.3 J/cm^2 had the highest energy among the LAP conditions, the other conditions had lower activated dopant concentrations.

This indicates that the lower powered LAPs are not suitable even though they seem to have a shallower doping profile in the SIMS results.

Directly measuring the LAP temperature curve is even more difficult than with FLP due to its very fast process time (50 ns). For this reason, we also made predictions of the temperature generated by a pulsed laser. The LAP thermal simulation results are provided in Fig. 4c by depth (0 nm, 10 nm, 100 nm, 1 μm) from the surface to the bottom of the substrate. The figure plots the graph in detail again to illustrate the temperature in the short time period.

According to the thermal simulation results, the LAP with the blue conditions (energy density: 0.3 J/cm^2) raised the surface temperature to 1,100 °C in a very short time; the temperature transition with the pulsed laser only took 50 nanoseconds. The graph below shows that there is a relatively shallow isothermal layer (surface $\sim$ 10 nm) and this indicates that the dopants will make a shallower activation layer; the dopants will diffuse less and the thermal energy needed for dopant activation will only be localized near the surface.

The SRP results in Fig. 4b supports these results. The junction depth for the LAP was 10 nm and the P concentration decreased dramatically with more depth. These results experizmentally prove that shallower junctions were formed by the annealing process with the shorter lamp duration. Finally, using the LAP, a USJ of about 10 nm was obtained, while the RTP and FLP showed a relatively deeper junction. Our results also revealed that the maximum activation level was relatively low. The reason was that the laser activation annealed the sample so fast that the total amount of dopants that driven-in was not enough to reach maximum solubility limit. However, the annealing duration of laser is so short that even more injected beams will not produce a deeper profile of dopants but we expect that it will drive-in and activate the dopants.

Materials can be modified to minimize SCEs. In this study, a Si_3N_4 layer was used as the capping layer to prevent the out-diffusion of dopants, and the layer also worked to trap heat at the surface. To make shallower junctions, below 5 nm, a capping layer with lower thermal diffusivity will enhance the thermal effect just at the surface. Since SCEs are induced by scaling mismatches, the importance of controlling electric field is being noted and the future devices will be developed [42]–[45].

IV. CONCLUSION

In conclusion, we achieved a USJ with n-type doping using P deposited by PaD and LAP. Our PaD with no bias power allowed damage-free dopant delivery without directionality effects. Our first attempted activation method, RTP, resulted in a relatively deep junction (> 35 nm) and low surface dopant concentration (2×10^{19} cm^{-3}). The RTP was successful at decreasing the junction depth with a shorter annealing time, but it was limited by the minimum lamp duration of the RTP process (a few seconds). Accordingly, we employed the FLP for our next attempt. The FLP produced a shallower junction (∼30 nm) than the RTP. However, the FLP depth was still at the tens of nanometer scale, while the expected depth needed for a USJ is about 10 nm.

Finally, the LAP was used to provide an extremely short annealing duration. The LAP raised the surface temperature to 1,100 °C in a very short time (50 ns) and formed an extremely shallow isothermal layer. The final SRP result for the LAP showed that a 10 nm deep USJ was formed, which indicates that the LAP with modified plasma assisted doping is a powerful method for fabricating USJs.

REFERENCES

[1] J. Kim, A. J. Hong, S. M. Kim, K.-S. Shin, E. B. Song, Y. Hwang, F. Xiu, K. Galatsis, C. O. Chui, R. N. Candler, S. Choi, J.-T. Moon, and K. L. Wang, "A stacked memory device on logic 3D technology for ultra-high-density data storage," *Nanotechnology*, vol. 22, no. 25, May 2011, Art. no. 254006.

[2] Y. Cho, Y. Hwang, H. Kim, E. Lee, S. Hong, H. Chung, D. Kim, J. Kim, Y. Oh, H. Hong, G.-Y. Jin, and C. Chung, "Novel deep trench Buried-Body-Contact (DBBC) of $4F^2$ cell for sub 30nm DRAM technology," in *Proc. Eur. Solid-State Device Res. Conf. (ESSDERC)*, Sep. 2012, pp. 193–196.

[3] B.-I. Choe, B.-G. Park, and J.-H. Lee, "Body doping profile of select device to minimize program disturbance in three-dimensional stack NAND flash memory," *Jpn. J. Appl. Phys*, vol. 52, no. 6S, Jun. 2013, Art. no. 06GE02.

[4] R. Jansen, "Silicon spintronics," *Nature Mater.*, vol. 11, no. 5, pp. 400–408, Apr. 2012.

[5] M. Fuechsle, J. A. Miwa, S. Mahapatra, H. Ryu, S. Lee, O. Warschkow, L. C. Hollenberg, G. Klimeck, and M. Y. Simmons, "A single-atom transistor," *Nature Nanotechnol.*, vol. 7, no. 4, pp. 242–246, Feb. 2012.

[6] *International Roadmap for Devices and Systems (IRDS)*. Accessed: Jun. 19, 2020. [Online]. Available: http://irds.ieee.org/

[7] K. Fuse, H. Tanimura, T. Aoyama, S. Kato, and I. Kobayashi, "Conformal SDE doping for FinFETs using an arsenic-doped sol-gel coating (SGC) and flash lamp annealing (FLA)," in *Proc. 17th Int. Workshop Junction Technol. (IWJT)*, Jun. 2017, pp. 66–68.

[8] J. Jang, H. S. Kim, W. Cho, H. Cho, J. Kim, S. I. Shim, J.-H. Jeong, B. K. Son, D. W. Kim, J. J. Shim, J. S. Lim, "Vertical cell array using TCAT (terabit cell array transistor) technology for ultra high density NAND flash memory," in *Proc. Symp. VLSI Technol.*, Jun. 2009, pp. 192–193.

[9] Y. Kim, H. Z. Massoud, and R. B. Fair, "The effect of ion-implantation damage on dopant diffusion in silicon during shallow-junction formation," *J. Electron. Mater.*, vol. 18, no. 2, pp. 143–150, Mar. 1989.

[10] R. Duffy, G. Curatola, B. J. Pawlak, G. Doornbos, K. van der Tak, P. Breimer, J. G. M. van Berkum, and F. Roozeboom, "Doping fin field-effect transistor sidewalls: Impurity dose retention in silicon due to high angle incident ion implants and the impact on device performance," *J. Vac. Sci. Technol. B, Microelectron. Nanometer Struct.*, vol. 26, no. 1, p. 402, Jan. 2008.

[11] R. F. Lever and K. W. Brannon, "A low energy limit to boron channeling in silicon," *J. Appl. Phys.*, vol. 69, no. 9, pp. 6369–6372, May 1991.

[12] G. Hobler, H.-H. Vuong, J. Bevk, A. Agarwal, H.-J. Gossmann, D. C. Jacobson, M. Foad, A. Murrell, and Y. Erokhin, "Modeling of ultra-low energy boron implantation in silicon," in *IEDM Tech. Dig.*, Washington, DC, USA, Dec. 1997, pp. 489–492.

[13] J. Woo Lee, Y. Sasaki, M. Ju Cho, M. Togo, G. Boccardi, R. Ritzenthaler, G. Eneman, T. Chiarella, S. Brus, N. Horiguchi, G. Groeseneken, and A. Thean, "Plasma doping and reduced crystalline damage for conformally doped fin field effect transistors," *Appl. Phys. Lett.*, vol. 102, no. 22, Jun. 2013, Art. no. 223508.

[14] H. Ueda, P. L. G. Ventzek, M. Oka, M. Horigome, Y. Kobayashi, Y. Sugimoto, T. Nozawa, and S. Kawakami, "Conformal doping of topographic silicon structures using a radial line slot antenna plasma source," *J. Appl. Phys.*, vol. 115, no. 21, Jun. 2014, Art. no. 214904.

[15] S. Baik, H. Kwon, C. Paeng, H. Zhang, B. Kalkofen, J. E. Jang, Y. S. Kim, and H.-J. Kwon, "Boosting n-type doping levels of ge with co-doping by integrating plasma-assisted atomic layer deposition and flash annealing process," *IEEE Electron Device Lett.*, vol. 40, no. 9, pp. 1507–1510, Sep. 2019.

[16] P. Baeri, S. U. Campisano, G. Foti, and E. Rimini, "A melting model for pulsing-laser annealing of implanted semiconductors," *J. Appl. Phys.*, vol. 50, no. 2, pp. 788–797, Feb. 1979.

[17] R. Duffy, T. Dao, Y. Tamminga, K. van der Tak, F. Roozeboom, and E. Augendre, "Groups III and v impurity solubilities in silicon due to laser, flash, and solid-phase-epitaxial-regrowth anneals," *Appl. Phys. Lett.*, vol. 89, no. 7, Aug. 2006, Art. no. 071915.

[18] K. C. Phillips, H. H. Gandhi, E. Mazur, and S. Sundaram, "Ultrafast laser processing of materials: A review," *Adv. Opt. Photonics.*, vol. 7, no. 4, pp. 684–712, Dec. 2015.

[19] P. Asoka-Kumar, H. J. Stein, and K. G. Lynn, "Detection of hydrogen-plasma-induced defects in Si by positron annihilation," *Appl. Phys. Lett.*, vol. 64, no. 13, pp. 1684–1686, Mar. 1994.

[20] S. J. Jeng, G. S. Oehrlein, and G. J. Scilla, "Hydrogen plasma induced defects in silicon," *Appl. Phys. Lett.*, vol. 53, no. 18, pp. 1735–1737, Oct. 1988.

[21] S. Nunomura, I. Sakata, and K. Matsubara, "Formation of electronic defects in crystalline silicon during hydrogen plasma treatment," *AIP Adv.*, vol. 9, no. 4, Apr. 2019, Art. no. 045110.

[22] D. Mathiot and J. C. Pfister, "Influence of the nonequilibrium vacancies on the diffusion of phosphorus into silicon," *J. Appl. Phys.*, vol. 53, no. 4, pp. 3053–3058, Apr. 1982.

[23] D. Mathiot and J. C. Pfister, "Dopant diffusion in silicon: A consistent view involving nonequilibrium defects," *J. Appl. Phys.*, vol. 55, no. 10, pp. 3518–3530, May 1984.

[24] T. Y. Tan and U. Gösele, "Point defects, diffusion processes, and swirl defect formation in silicon," *Appl. Phys. A, Solids Surf.*, vol. 37, no. 1, pp. 1–17, May 1985.

[25] P. M. Fahey, P. B. Griffin, and J. D. Plummer, "Point defects and dopant diffusion in silicon," *Rev. Mod. Phys.*, vol. 61, no. 2, p. 289, Apr. 1989.

[26] P. Voyles, D. Muller, J. Grazul, P. Citrin, and H.-J. Gossmann, "Atomic-scale imaging of individual dopant atoms and clusters in highly n-type bulk Si," *Nature.*, vol. 416, no. 6883, p. 826, Apr. 2002.

[27] S. P. Murarka, "Phosphorus out-diffusion during high temperature anneal of phosphorus-doped polycrystalline silicon and SiO_2," *J. Appl. Phys.*, vol. 56, no. 8, pp. 2225–2230, Oct. 1984.

[28] J.-P. Colinge, "Multiple-gate SOI MOSFETs," *Solid-State Electron.*, vol. 48, no. 6, pp. 897–905, Jun. 2004.

[29] I. Ferain, C. A. Colinge, and J.-P. Colinge, "Multigate transistors as the future of classical metal–oxide–semiconductor field-effect transistors," *Nature.*, vol. 479, no. 7373, p. 310, Nov. 2011.

[30] A. Benninghoven, F. G. Rüdenauer, and H. W. Werner, Eds., *Secondary Ion Mass Spectrometry*. New York, NY, USA: Wiley, 1987.

[31] J. C. C. Tsai, "Shallow phosphorus diffusion profiles in silicon," *Proc. IEEE*, vol. 57, no. 9, pp. 1499–1506, Sep. 1969.

[32] A. Bentzen, A. Holt, J. S. Christensen, and B. G. Svensson, "High concentration in-diffusion of phosphorus in Si from a spray-on source," *J. Appl. Phys.*, vol. 99, no. 6, Mar. 2006, Art. no. 064502.

[33] T. Clarysse, D. Vanhaeren, I. Hoflijk, and W. Vandervorst, "Characterization of electrically active dopant profiles with the spreading resistance probe," *Mater. Sci. Eng. R, Rep.*, vol. 47, nos. 5–6, pp. 123–206, Dec. 2004.

[34] M. Miyao, N. Yoshihiro, T. Tokuyama, and T. Mitsuishi, "Correlation between lattice damage and electrical activation of phosphorus-implanted silicon," *J. Appl. Phys.*, vol. 49, no. 4, p. 2573, Aug. 1978.

[35] G. Queirolo, "Incremental sheet resistance and spreading resistance: A comparison," *J. Vac. Sci. Technol. B, Microelectron. Nanometer Struct.*, vol. 10, no. 1, p. 408, Jan. 1992.
[36] R. M. Fleming, C. H. Seager, E. Bielejec, G. Vizkelethy, D. V. Lang, and J. M. Campbell, "Defect annealing in neutron and ion damaged silicon: Influence of defect clusters and doping," *J. Appl. Phys.*, vol. 107, no. 5, Mar. 2010, Art. no. 053712.
[37] J. Kim, S. W. Bedell, and D. K. Sadana, "Improved germanium n^+/p junction diodes formed by coimplantation of antimony and phosphorus," *Appl. Phys. Lett.*, vol. 98, no. 8, Feb. 2011, Art. no. 082112.
[38] H. H. Gatzen, V. Saile, and J. Leuthold, "Doping and surface modification," in *Micro and Nano Fabrication*. Berlin, Germany: Springer-Verlag, 2016, pp. 279–282.
[39] D. Bäuerle, "Thermal, photophysical, and photochemical processes," in *Laser Processing and Chemistry*. Berlin, Germany: Springer-Verlag, 2013, pp. 21–22.
[40] S. Shishiguchi, A. Mineji, T. Hayashi, and S. Saito, "Boron implanted shallow junction formation by high-temperature/short-time/high-ramping-rate(400 C/sec) RTA," in *Proc. Symp. VLSI Technol.*, vol. 1, Jan. 1997, pp. 89–90.
[41] C. M. Polley, W. R. Clarke, J. A. Miwa, G. Scappucci, J. W. Wells, D. L. Jaeger, M. R. Bischof, R. F. Reidy, B. P. Gorman, and M. Simmons, "Exploring the limits of N-type ultra-shallow junction formation," *ACS Nano*, vol. 7, no. 6, pp. 5499–5505, May 2013.
[42] N. Singh, A. Agarwal, L. K. Bera, T. Y. Liow, R. Yang, S. C. Rustagi, C. H. Tung, R. Kumar, G. Q. Lo, N. Balasubramanian, and D.-L. Kwong, "High-performance fully depleted silicon nanowire (diameter $\leq$ 5 nm) gate-all-around CMOS devices," *IEEE Electron Device Lett.*, vol. 27, no. 5, pp. 383–386, May 2006.
[43] C.-W. Lee, A. Afzalian, N. D. Akhavan, R. Yan, I. Ferain, and J.-P. Colinge, "Junctionless multigate field-effect transistor," *Appl. Phys. Lett.*, vol. 94, no. 5, Feb. 2009, Art. no. 053511.
[44] K. J. Kuhn, "Considerations for ultimate CMOS scaling," *IEEE Trans. Electron Devices*, vol. 59, no. 7, pp. 1813–1828, Jul. 2012.
[45] H. Mertens, R. Ritzenthaler, A. Hikavyy, M.-S. Kim, Z. Tao, K. Wostyn, S. A. Chew, A. De Keersgieter, G. Mannaert, and E. Rosseel, "Gate-all-around MOSFETs based on vertically stacked horizontal Si nanowires in a replacement metal gate process on bulk Si substrates," in *Proc. IEEE Symp. VLSI Technol.*, Honolulu, HI, USA, Jun. 2016, pp. 1–2.

SEUNGHUN BAIK received the B.S. degree in electronic engineering from Inha University, Incheon, South Korea, in 2018. He is currently pursuing the Ph.D. degree with the Department of Information and Communication Engineering, Daegu Gyeongbuk Institute of Science and Technology (DGIST). His research interests include the contact engineering using laser annealing system and an improvement on performance of electronic devices.

DONG-JAE KWON received the B.S. degree in optical engineering from the Kumoh National Institute of Technology (KIT), Gumi, South Korea, in 2019. He is currently pursuing the M.S degree with the Department of Information and Communication Engineering, Daegu Gyeongbuk Institute of Science and Technology (DGIST). His research interests include laser annealing process for improving the performance of electronic devices and laser induced oxidation for making a nucleation site.

HONGKI KANG received the B.S. degree in electrical engineering from KAIST, Daejeon, South Korea, in 2008, and the M.S. and Ph.D. degrees in electrical engineering and computer sciences from the University of California at Berkeley, Berkeley, CA, USA, in 2010 and 2013, respectively. He is currently an Assistant Professor with the Department of Information and Communication Engineering, DGIST, Daegu, South Korea. His current research interests include flexible transparent bioelectronics, neural interfaces, and printing-based additive microfabrication.

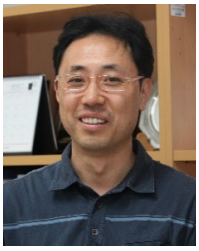

JAE EUN JANG (Member, IEEE) received the Ph.D. degree in electrical engineering from the University of Cambridge, Cambridge, U.K., in 2006. From 2007 to 2011, he was a Principal Senior Researcher with the Samsung Advanced Institute of Technology, Yongin, South Korea. Since 2011, he has been a Professor of Information and Communication Engineering with the Daegu Gyeongbuk Institute of Science and Technology (DGIST), Daegu, South Korea. He first demonstrated the mechanical nanoswitch and mechanical DRAM concept using vertically aligned carbon nanotubes, in 2004 and 2008. His current research interests include nanodevices for communication purposes and biomimic sensors.

JAEWON JANG (Member, IEEE) received the B.S. and master's degrees in electrical engineering from Korea University, Seoul, South Korea, in 2006 and 2008, respectively, and the Ph.D. degree from the Department of Electrical Engineering and Computer Sciences, University of California at Berkeley, CA, USA, in 2013. He is currently an Assistant Professor with the School of Electronics Engineering, Kyungpook National University, Daegu, South Korea.

Y. S. KIM is currently the Senior Director of Lam Research, Fremont, USA. As a Technical Expert, he has more than 30 years of experience in semiconductor industry including, five years in plasma material technology and nine years in applied materials to develop process technologies and various plasma reactors. In 2002, he joined Lam Research, where he has led and developed various technologies on both process and hardware for etch/clean and dep. He holds more than 70 U.S. patents.

HYUK-JUN KWON received the B.S. degree in mechanical engineering from Korea University, in 2007, the M.S. degree in mechanical engineering (MEMS) from KAIST, in 2009, and the Ph.D. degree with a designated emphasis in nanoscale science and engineering from the University of California at Berkeley, in August 2015. Then, he worked with the Samsung Advanced Institute of Technology (SAIT), for two years. He held a Postdoctoral Fellowship with the University of California at Berkeley, for five months. Since August 2017, he has been with Lam Research, Fremont, CA, USA. In September 2017, he joined the Department of Information and Communication Engineering, DGIST, as an Assistant Professor, where his research concerned the future semiconductor manufacturing equipment and processes, next-generation electrical devices with flexible/wearable platform, and laser processing.